Article

Description of Molecular Dynamics in Intense Laser Fields by the Time-Dependent Adiabatic State Approach: Application to Simultaneous Two-Bond Dissociation of CO and Its Control

Yukio Sato, Hirohiko Kono, Shiro Koseki, and Yuichi Fujimura

J. Am. Chem. Soc., **2003**, 125 (26), 8019-8031• DOI: 10.1021/ja0344819 • Publication Date (Web): 05 June 2003

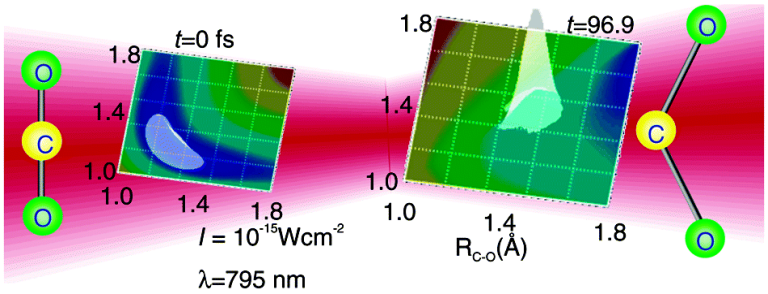

More About This Article

Additional resources and features associated with this article are available within the HTML version:

- Supporting Information
- Links to the 5 articles that cite this article, as of the time of this article download
- Access to high resolution figures
- Links to articles and content related to this article
- Copyright permission to reproduce figures and/or text from this article

View the Full Text HTML

J|A|C|S
ARTICLES
Published on Web 06/05/2003

Description of Molecular Dynamics in Intense Laser Fields by the Time-Dependent Adiabatic State Approach: Application to Simultaneous Two-Bond Dissociation of CO_2 and Its Control

Yukio Sato,[†] Hirohiko Kono,*[,†] Shiro Koseki,[‡] and Yuichi Fujimura[†]

Contribution from the Department of Chemistry, Graduate School of Science, Tohoku University, Sendai 980-8578, Japan, and College of Integrated Arts and Sciences, Osaka Prefecture University, Sakai, Osaka 599-8531, Japan

Received February 4, 2003; E-mail: kono@mcl.chem.tohoku.ac.jp

Abstract: We theoretically investigated the dynamics of structural deformations of CO_2 and its cations in near-infrared intense laser fields ($\sim 10^{15}$ W cm^{-2}) by using the time-dependent adiabatic state approach. To obtain "field-following" adiabatic potentials for nuclear dynamics, the electronic Hamiltonian including the interaction with the instantaneous laser electric field is diagonalized by the multiconfiguration self-consistent-field molecular orbital method. In the CO_2 and CO_2^+ stages, ionization occurs before the field intensity becomes high enough to deform the molecule. In the CO_2^{2+} stage, *simultaneous* symmetric *two-bond* stretching occurs as well as one-bond stretching. Two-bond stretching is induced by an intense field in the lowest time-dependent adiabatic state $|1\rangle$ of CO_2^{2+}, and this two-bond stretching is followed by the occurrence of a large-amplitude bending motion mainly in the second-lowest adiabatic state $|2\rangle$ nonadiabatically created at large internuclear distances by the field from $|1\rangle$. It is concluded that the experimentally observed stretched and bent structure of CO_2^{3+} just before Coulomb explosions originates from the structural deformation of CO_2^{2+}. We also show in this report that the concept of "optical-cycle-averaged potential" is useful for designing schemes to control molecular (reaction) dynamics, such as dissociation dynamics of CO_2, in intense fields. The present approach is simple but has wide applicability for analysis and prediction of electronic and nuclear dynamics of polyatomic molecules in intense laser fields.

1. Introduction

The development of high-power lasers has opened frontiers of science on light−matter interaction, which cover a broad area of atomic and molecular sciences.[1,2] Handy laser systems of high intensity have been used for various applications such as precise material processing and medical application. The advent of such light sources has made a new tool for manipulating the dynamics of molecules on an ultrashort time scale available to chemists.[3,4] In intense fields ($I > 10^{13}$ W/cm^2), the Coulombic potentials that the electrons are placed in are greatly distorted:[5−7] a large part of the electron density is transferred among nuclei within a half optical cycle ($\sim$1.3 fs for $\lambda = 800$ nm light).[8−10] A light intensity of 1 au, i.e., 3.5×10^{16} W/cm^2, exerts on an electron a force that is as strong as the electron−nucleus interaction in a hydrogen atom. Laser-induced intramolecular electron transfer triggers nuclear motion. It should be emphasized that the interaction of an intense field with molecules is not restricted to resonant electronic or vibrational transitions. Strong-field, near-infrared pulses (centered around $\sim$800 nm) can induce chemical reactions[3,4] or structural deformations such as bond stretching and bond angle bending, for example, as observed by Yamanouchi et al. for CO_2.[11]

The resultant structural deformations in turn change the electronic response to the field, e.g., the efficiency of intramolecular electron transfer and the probability of tunnel type of ionization, in which an electron penetrates (or goes beyond) the distorted barrier(s) for ionization. For tunnel type ionization,[5−7,12] as the field becomes stronger and its period, $2\pi/\omega$, becomes longer, an electron can be ejected from the molecule before the phase of the field changes. It is known that tunnel ionization is greatly enhanced at a critical internuclear distance, R_c, which is much longer than the equilibrium internuclear distance, R_e

[†] Tohoku University.
[‡] Osaka Prefecture University.

(1) Yamanouchi, K. *Science* **2002**, *295*, 1659−1660.
(2) *Laser Control and Manipulation of Molecules*; Bandrauk, A. D., Gordon, R. J., Fujimura, Y., Eds.; ACS Symposium Series Vol. 821; Oxford University Press: Oxford, 2002.
(3) Assion, A.; Baumert, T.; Bergt, M.; Brixner, T.; Kiefer, B.; Seyfried, V.; Strehle, M.; Gerber, G. *Science* **1998**, *282*, 919−922.
(4) Levis, J. R.; Menkir, G. M.; Rabitz, H. *Science* **2001**, *292*, 709−713.
(5) Keldysh, L. V. *Sov. Phys. JETP* **1965**, *20*, 1307−1314.
(6) Faisal, F. H. M. *J. Phys. B* **1973**, *6*, L89−92. Augst, S.; Meyerhofer, D. D.; Strickland, D.; Chin, S. L. *J. Opt. Soc. Am. B* **1991**, *8*, 858−867. Ammosov, M. V.; Delone, N. B.; Krainov, V. P. *Sov. Phys. JETP* **1986**, *64*, 1191−1194.
(7) Krainov, V. P.; Reiss, H. R.; Smirnov, B. M. *Radiative Processes in Atomic Physics*; Wiley: New York, 1997.
(8) Kawata, I.; Kono, H.; Fujimura, Y. *J. Chem. Phys.* **1999**, *110*, 11152−11165. Kawata, I.; Kono, H.; Fujimura, Y. *Chem. Phys. Lett.* **1998**, *289*, 546−552.
(9) Harumiya, K.; Kawata, I.; Kono, H.; Fujimura, Y. *J. Chem. Phys.* **2000**, *113*, 8953−8960.
(10) Lezius, M.; Blanchet, V.; Ivanov, M.; Yu.; Stolow, A. *J. Chem. Phys.* **2002**, *117*, 1575−1588.
(11) Hishikawa, A.; Iwamae, A.; Yamanouchi, K. *Phys. Rev. Lett.* **1999**, *83*, 1127−1130.
(12) DeWitt, M. J.; Levis, R. J. *J. Chem. Phys.* **1998**, *108*, 7739−7742.

(known as enhanced ionization).[13−17] Enhanced ionization has been experimentally observed for various molecules,[14−17] such as CO_2 and benzene molecules.[11,18] The correlation between ionization and structural deformation is thought to play a decisive role in fragmentation and reaction processes.[19−21]

Attempts to use intense laser pulses for controlling chemical reactions have recently begun. Gerber et al. used near-infrared, intense femtosecond laser pulses tailored by a genetic algorithm-controlled pulse shaper to optimize the branching ratios of different organometallic photodissociation channels.[3] Levis et al. recently reported selective bond dissociation and rearrangement of polyatomic molecules, such as acetophenone, by optically tailored, intense-field laser pulses ($\sim 10^{14}$ W/cm^2).[4] Many excited states that are dynamically Stark-shifted by such intense pulses can open various channels for reactions, and reaction selectivity is achieved by optimizing the phases and amplitudes of the optical component frequencies with a liquid crystal light modulator in the pulse shaper. However, it is a very difficult task to experimentally determine in which stage the structural deformations or chemical reactions occur, e.g., while the molecule is neutral or while it is a monocation. Furthermore, to enhance reaction selectivity, the mechanisms and characteristic features of molecular (electronic and nuclear) dynamics in intense fields must be elucidated. To the best of our knowledge, there were no practical, unified theoretical treatments to explain both electronic and nuclear dynamics of polyatomic molecules in intense laser fields. There is therefore an urgent need for the development of theoretical approaches to deal with dynamics in intense fields.

In previous studies,[8,9,22] we have accurately solved the time-dependent Schrödinger equations of H_2^+ and H_2 by using an efficient grid-point wave packet method based on the dual transformation technique.[23] The calculated electronic and nuclear dynamics is analyzed by using "field-following" adiabatic states $\{|n\rangle\}$ defined as eigenfunctions of the "instantaneous" electronic Hamiltonian $H_{el}(t)$ including the interaction with a laser electric field $\epsilon(t)$.[8,22,24−27] Only field-free adiabatic states, i.e., bound state components, are used to diagonalize $H_{el}(t)$. The analysis has shown that the nuclear dynamics in a near-infrared field can be described in terms of wave packet propagation on time-dependent adiabatic potentials and nonadiabatic transitions due to temporal change in $\epsilon(t)$. It also turns out that tunnel ionization occurs from an adiabatic state or adiabatic states to Volkov states[7] (quantum states of a free electron in a laser field). The important concept "doorway state to tunnel ionization" is thus introduced. The charge distributions on individual atomic sites of doorway states to ionization can be used to judge whether ionization occurs or not at a given intensity.

The purpose of this study is to demonstrate that the above description of dynamics in terms of "field-following" adiabatic states, i.e., the time-dependent adiabatic state approach, is useful for analyzing and predicting the *electronic* and *nuclear* dynamics of *polyatomic* molecules in intense laser fields. The properties of the adiabatic states of polyatomic molecules can be calculated by ab initio molecular orbital (MO) methods.[28] In this study, we apply the proposed approach to dynamics of CO_2 in near-infrared intense fields, since reliable experimental data of field-induced structural deformation of CO_2 is now available,[11] as mentioned in the next paragraph. From the results of calculation of the nuclear wave packet dynamics of CO_2 and its cations, we extract characteristic features of the dynamics of CO_2 in intense fields that are responsible for the structural deformation. We also propose a scheme to control bond breaking of CO_2 species by using a two-color pulse of ω and 2ω.

In an intense field, cations created are successively ionized at large internuclear distances (due to enhanced ionization), and resultant multiply charged cations undergo Coulomb explosions (due to repulsion among positively charged atomic sites).[11,14−17] On the basis of distribution patterns in a covariance map of fragment ions,[29] Cornaggia studied the geometrical structures of CO_2 cations that are about to Coulomb explode and suggested the existence of a large amplitude bending motion.[30] The structures of created cations can now be precisely determined by measuring the momentum vector distributions with mass-resolved momentum imaging[31] and coincidence momentum imaging,[32] which are considered useful techniques for obtaining snapshots of the spatial configuration of a molecule. By using these momentum imaging techniques, Hishikawa et al. investigated the geometrical structure of exploding CO_2^{3+} in a 1.1 PW cm^{-2}, 100-fs pulse ($\lambda = 795$ nm) and found that the C−O bond length is stretched to about 1.7 Å and that the mean amplitude of bending is large (the mean bending angle from linear geometry being $\sim 20°$).[11] However, the deformation stage, i.e., the stage in which deformation of the structure of exploding cations is induced, has not been experimentally determined yet. In this paper, we reveal the origin of the structural deformation of exploding CO_2^{3+}.

(13) Zuo, T.; Bandrauk, A. D. *Phys. Rev. A* **1993**, *48*, 3837. Bandrauk, A. D. *Comments At. Mol. Phys. D* **1999**, *1*, 97−115. Seidemann, T.; Ivanov, M. Y.; Corkum, P. B. *Phys. Rev. Lett.* **1995**, *75*, 2819−2822.
(14) Gibson, G. N.; Li, M.; Guo, C.; Nibarger, J. P. *Phys. Rev. A* **1998**, *58*, 4723−4727.
(15) Posthumus, J. H.; Giles, A. J.; Thompson, M. R.; Codling, K. *J. Phys. B* **1996**, *29*, 5811−5830. Codling, K.; Frasinski, L. J. *J. Phys. B* **1993**, *26*, 783−810.
(16) Constant, E.; Stapelfelt, H.; Corkum, P. B. *Phys. Rev. Lett.* **1996**, *76*, 4140−4143.
(17) Schmidt, M.; Normand, D.; Cornaggia, C. *Phys. Rev. A* **1994**, *50*, 5037−5045.
(18) Shimizu, S.; Kou, J.; Kawato, S.; Shimizu, K.; Sakabe, S.; Nakashima, N. *Chem. Phys. Lett.* **2000**, *317*, 609−614.
(19) Harada, H.; Shimizu, S.; Yatsuhashi, T.; Sakabe, S.; Izawa, Y.; Nakashima, N. *Chem. Phys. Lett.* **2001**, *342*, 563−570.
(20) Itakura, R.; Watanabe, J.; Hishikawa, A.; Yamanouchi, K. *J. Chem. Phys.* **2001**, *114*, 5598−5606.
(21) Robson, L.; Ledingham, K. W. D.; Tasker, A. D.; McKenna, P.; McCanny, T.; Kosmidis, C.; Jaroszynski, D. A.; Jones, D. R.; Issac, R. C.; Jamieson, S. *Chem. Phys. Lett.* **2002**, *360*, 382−389.
(22) Harumiya, K.; Kono, H.; Fujimura, Y.; Kawata, I.; Bandrauk, A. D. *Phys. Rev. A* **2002**, *66*, 043403−1−14.
(23) Kawata, I.; Kono, H. *J. Chem. Phys.* **1999**, *111*, 9498−9508. Kono, H.; Kita, A.; Ohtsuki, Y.; Fujimura, Y. *J. Comput. Phys.* **1997**, *130*, 148−159.
(24) Kono, H.; Koseki, S. In ref 2, pp 267−284.
(25) Kono, H.; Kawata, I. In *Advances in Multi-Photon Processes and Spectroscopy*; Gordon, R. J., Fujimura, Y., Eds.; World Scientific: Singapore, 2001; Vol. 14, pp 165−188.
(26) Kono, H.; Harumiya, K.; Fujimura, Y.; Kawata, I. In *Photonic, Electronic and Atomic Collisions* (*XXII ICPEAC*), Burgdorfer, J., Cohen, J., Datz, S., Vane, C. R., Eds.; Rinton: Princeton, NJ, 2001; pp 197−208. Kono, H.; Sato, Y.; Fujimura, Y.; Kawata, I. *Laser Phys.* **2003**, in press.
(27) Kawata, I.; Kono, H.; Fujimura, Y.; Bandrauk, A. D. *Phys. Rev. A* **2000**, *62*, 031401(R)1-4. Kawata, I.; Bandrauk, A. D.; Kono, H.; Fujimura, Y. *Laser Phys.* **2001**, *11*, 188−197.
(28) Kono, H.; Koseki, S.; Shiota, M.; Fujimura, Y. *J. Phys. Chem. A* **2001**, *105*, 5627−5636.
(29) Frasinski, L. J.; Codling, K.; Hatherly, P. A. *Science* **1989**, *246*, 1029−1031. Card, D. A.; Wisniewski, E. S.; Folmer D. E.; Castleman, A. W., Jr. *Int. J. Mass Spectrosc.* **2003**, *223−224*, 355−363.
(30) Cornaggia, C. *Phys. Rev. A* **1993**, *54*, R2555−2558.
(31) Iwamae, A.; Hishikawa, K.; Yamanouchi, K. *J. Phys. B* **2000**, *33*, 223−240.
(32) Hasegawa, H.; Hishikawa, K.; Yamanouchi, K. *Chem. Phys. Lett.* **2001**, *349*, 57−63.

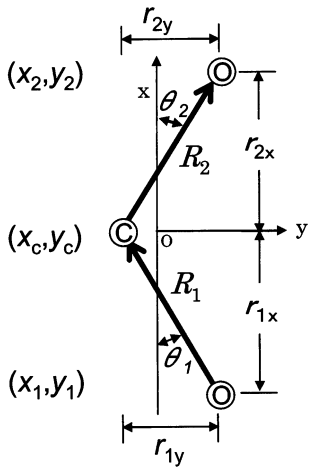

Figure 1. Coordinates of a triatomic molecule CO_2 on the $x-y$ plane. The Cartesian coordinates of the C atom are denoted by (x_C, y_C), and those of the jth O atom are denoted by (x_j, y_j). The relative coordinates {r_{1x}, r_{2x}, r_{1y},r_{2y}} are defined as $r_{1x} = x_C - x_1$, $r_{2x} = x_2 - x_C$, $r_{1y} = y_C - y_1$, and $r_{2y} = y_2 - y_C$; R_1 and R_2 denote the lengths of the two C−O bonds. The angle between the x-axis and a C−O bond direction is denoted by θ_1 or θ_2.

2. Description of Dynamics in Intense Laser Fields by Time-Dependent Adiabatic States

We present an outline of a time-dependent adiabatic state approach to study dynamics of a polyatomic molecule CO_2 in intense fields. To obtain the time-dependent adiabatic potential surfaces of CO_2, we construct the instantaneous electronic Hamiltonian $H_{el}(t)$ as follows. As shown in Figure 1, the three atoms O, C, and O of CO_2 are designated by 1, C, and 2, respectively. The Cartesian coordinates of the C atom are denoted by (x_c, y_c, z_c), and those of the jth O atom are denoted by (x_j, y_j, z_j). The nuclear charges of O and C atoms are denoted by e_O and e_C, respectively. The applied laser electric field $\epsilon(t)$ is assumed to be polarized parallel to the x-axis. In a long-wavelength case, the interaction with $\epsilon(t)$ can be expressed by the dipole interaction

$$-[-e(\sum_i x_{e,i}) + e_O x_1 + e_O x_2 + e_C x_C]\,\epsilon(t) = -[-e(\sum_i (x_{e,i} - X)) + e_O(x_1 - X) + e_O(x_2 - X) + e_C(x_C - X)]\,\epsilon(t) - QX\,\epsilon(t) \equiv -\mu_{int}\epsilon(t) - QX\,\epsilon(t) \quad (1)$$

where $x_{e,i}$ is the x coordinate of the ith electron, X is the x component of the center of mass of the molecule, and Q is the total charge of the molecule (for instance, $Q = +2$ for a dication). The difference from X, for instance, ($x_{e,j} - X$) or ($x_C - X$), can be expressed in terms of appropriate relative coordinates. In the dipole approximation, therefore, the center of mass can be separated from the internal degrees of freedom. The center of mass of the molecule moves in a field potential $-QX\,\epsilon(t)$ as a particle with the total mass and total charge $+Q$ of the whole molecule; the term $-QX\,\epsilon(t)$ should not be included in the Hamiltonian for the internal degrees of freedom.

In the following derivation of internal Hamiltonians and MO calculations, the center of mass, (X,Y,Z), is assumed to be equal to the center of the nuclei, (X',Y',Z'), because the difference is negligible in the present problem. Thus, the coordinates of the ith electron are given by the relative coordinates ($x_{e,j} - X'$, $y_{e,j} - Y'$, $z_{e,j} - Z'$); the nuclear coordinates are measured from (X',Y',Z') and can be expressed in terms of internal (vibrational) coordinates and molecular rotation denoted by a set {R}. We hence can define the instantaneous electronic Hamiltonian $H_{el}(\{R\},t) = H_{el}(t)$ by adding $-\mu_{int}\epsilon(t)$ to the field-free adiabatic electronic Hamiltonian $H_{el}(\{R\},\epsilon(t)=0)$ as

$$H_{el}(\{R\},t) = H_{el}(\{R\},\epsilon(t)=0) - \mu_{int}\,\epsilon(t) \quad (2)$$

In diagonalization of the instantaneous electronic Hamiltonian $H_{el}(\{R\},t)$, both {R} and t are treated as adiabatic parameters

$$H_{el}(\{R\},t)\,\psi(\{R\},t) = V(\{R\},t)\,\psi(\{R\},t) \quad (3)$$

The eigenvalues $V(\{R\},t)$ are time-dependent adiabatic potentials for nuclear motion.

In a previous study,[28] we solved eq 3 of CO_2 and its cations at various instantaneous field strengths by using MO methods and found that the multiconfiguration self-consistent-field (MCSCF) method is reliable for the present problem. The adiabatic potential surfaces $V(\{R\},t)$ and wave functions $\psi(\{R\},t)$ used in this paper are calculated by using the full-optimized reaction space MCSCF method[33]with the 6-311+G(d) basis set.[34] The MCSCF active space contains all of the valence orbitals and valence electrons of CO_2 and its cations. For a nonzero field case, the MOs and the expansion coefficients of the configuration state functions are optimized by incorporating the dipole interaction $-\mu_{int}\epsilon(t)$ with a static field into the Hamiltonian of the MCSCF method. All ab initio MO calculations are performed using the GAMESS suite of program codes.[35]

In a high-intensity regime, field-following adiabatic potential surfaces can cross each other in energy (avoided level crossing), resulting in the occurrence of nonadiabatic transitions between adiabatic states.[36] Nonadiabatic transition caused by the temporal change in $\epsilon(t)$ is characteristic of dynamics in intense fields. The field-induced nonadiabatic coupling between two time-dependent adiabatic states $\psi_a(t)$ and $\psi_b(t)$ is given by $\langle\psi_a(t)|\partial/\partial t|\psi_b(t)\rangle$. The coupling can be easily evaluated from the following convenient form obtained by differentiating $H_{el}(t)\psi_a(t) = E_a(t)\psi_a(t)$ and $H_{el}(t)\psi_b(t) = E_b(t)\psi_b(t)$ with respect to time t

$$\langle\psi_a(t)|\partial/\partial t|\psi_b(t)\rangle = \mu_{ab}(t)[\partial\epsilon(t)/\partial t]/[E_b(t) - E_a(t)] \quad (4)$$

where μ_{ab} is the polarization direction component of the electronic transition moment between $\psi_a(t)$ and $\psi_b(t)$. Nonadiabatic transitions are dominant if the energy gap $E_b(t) - E_a(t)$ is smaller than the coupling $\langle\psi_a(t)|\partial/\partial t|\psi_b(t)\rangle$ at the avoided crossing. According to the Landau−Zener formula,[36,37] the nonadaiabatic transition probability is given by

$$P_{ab} = e^{-\pi\delta/4} \quad (5)$$

(33) Ruedenberg, K.; Schmidt, M. W.; Dombek, M. M.; Elbert, S. T. *Chem. Phys.* **1982**, *71*, 41−50, 51−64, 65−78. Schmidt, M. W.; Gordon, M. S. *Annu. Rev. Phys. Chem.* **1998**, *49*, 233−266.
(34) Krishnan, R.; Binkley, J. S.; Seeger, R.; Pople, J. A. *J. Chem. Phys.* **1980**, *72*, 650−654.
(35) Schmidt, M. W.; Baldridge, K. K.; Boatz, J. A.; Elbert, S. T.; Gordon, M. S.; Jensen, J. H.; Koseki, S.; Matsunaga, N.; Nguyen, K. A.; Su, S.; Windus, T. L.; Dupuis, M.; Montgomery, J. A., Jr. *J. Comput. Chem.* **1993**, *14*, 1347−1363.
(36) Kayanuma, Y. *Phys. Rev. A* **1994**, *50*, 843−845.
(37) Zener, C. *Proc. R. Soc. London, Ser. A* **1932**, *137*, 696−702. Zhu, C.; Teranishi, Y.; Nakamura, H. *Adv. Chem. Phys.* **2001**, *117*, 127−233.

where δ is the ratio $|[E_b(t) - E_a(t)]/\langle\psi_a(t)|\partial/\partial t|\psi_b(t)\rangle|$ evaluated at the avoided crossing.

Determination of the characteristic features of electronic dynamics of H_2^+ and H_2 molecules in an intense laser field has led to the simple electrostatic view that each atom in a molecule is charged by field-induced electron transfer and that ionization proceeds via the most unstable (most negatively or least positively charged) atomic site.[8,22,24−27] We have shown that the doorway state to ionization in H_2 is the lowest adiabatic state characterized by a charge-transferred localized ionic state H^+H^- or H^-H^+.[9,22] As in previous papers, we derive a criterion for ionization based on electrostatic consideration.[38] It is known that the tunnel ionization rate has a maximum at the geometry in which the molecular axis is parallel to the polarization direction.[39,40] As the most important spatial configuration, we next consider a linear CO_2 molecule with charges O^{Q_1+} C^{Q_C+} O^{Q_2+} placed parallel to $\epsilon(t)$.

In the lowest adiabatic state of CO_2, when a field is applied, an appreciable amount of negative charge is transferred from O atom to O atom in the direction that the instantaneous dipole interaction energy of the electrons becomes lower. Results of numerical calculations indicate that the charge on the C atom changes only a little in an intense field.[28] Therefore, another electronic configuration to consider is the field-induced charge-transfer ionic component $O^{(Q_1-1)+}$ C^{Q_C+} $O^{(Q_2+1)+}$. In an intense field, the two adiabatic states represented by O^{Q_1+} C^{Q_C+} O^{Q_2+} and $O^{(Q_1-1)+}$ C^{Q_C+} $O^{(Q_2+1)+}$ come close to each other in energy. Near the avoided crossing, the component $O^{(Q_1-1)+}$ C^{Q_C+} $O^{(Q_2+1)+}$ becomes dominant in the lowest adiabatic state. From the difference in electrostatic energy between the two configurations, the field strength, ϵ_c, required for the creation of $O^{(Q_1-1)+}$ C^{Q_C+} $O^{(Q_2+1)+}$ due to avoided crossing, is then given by[28]

$$\epsilon_c = [I_p(O^{Q_2+} - I_p(O^{(Q_1-1)+}) - (Q_2 + 1 - Q_1)/R_{O-O}]\}/R_{O-O} \quad (6)$$

where R_{O-O} is the O−O bond length and $I_p(O^{Q_j+})$ is the ionization potential of an O atom with charge $+Q_j$. Although the ionization probability may depend on the details of the electronic character such as spin multiplicity, the estimated value of ϵ_c is regarded as the value of the intensity required for tunnel ionization because the charge transfer ionic state is electronically unstable and is hence expected to be a doorway state to tunnel ionization. It is confirmed that the electrostatic model as represented by eq 6 is valid in the case of H_2.[9,22]

3. Derivation of Vibrational Hamiltonians of CO_2 in Intense Fields

We denote the mass of a C atom by m_C and that of an O atom by m_O. After separating the center of mass from the total nuclear system, we obtain the kinetic energy for the internal nuclear degrees of freedom as follows

$$\hat{T} = \sum_{l=x,y,z}\left\{-\frac{\hbar^2}{2\mu}\left(\frac{\partial^2}{\partial r_{1l}^2} + \frac{\partial^2}{\partial r_{2l}^2}\right) + \frac{\hbar^2}{m_C}\frac{\partial^2}{\partial r_{1l}\partial r_{2l}}\right\} \quad (7)$$

where the reduced mass μ is given by $\mu = \{m_C m_O\}/\{(m_C + m_O)\}$ and the relative coordinates $\{r_{1x}, r_{2x}, r_{1y}, r_{2y}, r_{1z}, r_{2z}\}$ are defined as $r_{1x} = x_C - x_1$, $r_{2x} = x_2 - x_C$, . . ., as shown in Figure 1.

In the following, we assume that the molecule does not rotate during the interaction with a laser pulse. A linearly polarized intense laser field can align molecules.[41] The rotational motion of a molecule cannot follow the rapid optical oscillation of $\epsilon(t)$ but can follow the change in a slowly varying electric field envelope $f(t)$. The effective potential for molecular rotation of a linear molecule is known to be[42]

$$-(\alpha_{xx} - \alpha_{yy})(\cos\chi)^2 f^2(t)/4 \quad (8)$$

where χ is the angle between the molecular axis and the polarization direction of the field $\epsilon(t)$ and α_{xx} and α_{yy} are the molecular axis component and perpendicular component of the polarizability, respectively. For the experimentally determined value $\alpha_{xx} - \alpha_{yy} = 13.8$ au,[43] the potential depth of CO_2 is about 0.15 eV (∼1200 cm^{-1}) at $I \approx 3 \times 10^{13}$ W cm^{-2}. Above this intensity, the appearance of CO_2^+ is experimentally confirmed.[44] The field strength $\epsilon(t)$ in atomic units corresponds to $(5.14 \times 10^{11})\epsilon(t)$ V m^{-1} in SI units, and the field envelope $f(t)$ in atomic units corresponds to the light intensity $I = (3.5 \times 10^{16})f^2(t)$ W cm^{-2}. The depth of (∼1200 cm^{-1}) is sufficiently large to align CO_2 at room temperature. However, to achieve a high degree of alignment in the polarization direction by adiabatic following of the molecular rotation to the pulse envelope, the pulse duration must be longer than the time scale of rotational motion, i.e., $2\pi/2B \approx 40$ ps, where B (≈0.39 cm^{-1}) is the rotational constant of CO_2 .[40,45] Since the pulse duration used in the experiment (≈100 fs) is much shorter than $2\pi/2B$, the alignment is incomplete.

Without rotation, the degrees of freedom of a CO_2 molecule are reduced to 4 vibrational modes, namely, two bond stretching modes and two degenerate modes for bond angle bending. It is still time-consuming to construct potential surfaces for these four vibrational degrees of freedom. In this paper, we select two degrees of freedom from among them and derive two effective vibrational Hamiltonians that are suitable for describing the nuclear dynamics of CO_2 in intense fields. The first one is constructed from the two bond-stretching modes of CO_2 in the case of linear geometry, and the second one is constructed from the symmetric bond stretching and bond angle bending modes.

A. One-Dimensional Space (Linear Geometry Case). First, we assume that the molecule is linear and is aligned parallel to the polarization direction x: $r_{1y} = r_{2y} = r_{1z} = r_{2z} = 0$. (No bending is taken into account.) In this case, r_{1x} and r_{2x} can be replaced with the O−C bond length R_1 and C−O bond length

(38) Bandrauk, A. D. In *The Physics of Electronic and Atomic Collisions*; Itikawa, Y., et al., Eds.; AIP Conf. Proc. 500; American Institute of Physics: New York, 1999; pp 102−117.
(39) Posthumus, J. H.; Plumridge, J.; Frasinski, L. J.; Codling, K.; Langley, A. J.; Tady, P. F. *J. Phys. B* **1998**, *31*, L985−993. Ellert, C.; Corkum, P. B. *Phys. Rev. A* **1999**, *59*, R3170−3173.
(40) Banerjee, S.; Kumar, G. R.; Mathur, D. *Phys. Rev. A* **1999**, *60*, R3369−3372.
(41) Larsen, J. J.; Sakai, H.; Safvan, C. P.; Wendt-Larsen, Ida; Stapelfeldt, H. *J. Chem. Phys.* **1999**, *111*, 7774−7781. Schmidt, M.; Dobosz, S.; Meynadier, P.; D'Oliveira, P.; Normand, D.; Charron, E.; Suzor-Weiner, A. *Phys. Rev. A* **1999**, *60*, 4706−4714.
(42) Friedrich, B.; Herschbach, D. *Phys. Rev. Lett.* **1995**, *74*, 4623−4626. Keller, A. *J. Mol. Structure* (*THEOCHEM*) **1999**, *493*, 103−115.
(43) Spackman, M. A. *J. Phys. Chem.* **1989**, *93*, 7594−7603.
(44) Cornaggia, C.; Hering, P. *Phys. Rev. A* **2000**, *62*, 023403−1−13.
(45) Origoso, J.; Rodríguez, M.; Gupta, M.; Friedrich, B. *J. Chem. Phys.* **1999**, *110*, 3870. Mathur, D.; Banerjee, S.; Ravindra Kumar, G. In ref 2, pp 336−349.

R_2, respectively. From the x component in eq 7, we obtain the vibrational kinetic energy in the case of linear geometry[46]

$$\hat{T}_x = -\frac{\hbar^2}{2\mu}\left(\frac{\partial^2}{\partial {R_1}^2} + \frac{\partial^2}{\partial {R_2}^2}\right) + \frac{\hbar^2}{m_C}\frac{\partial^2}{\partial R_1 \partial R_2} \tag{9}$$

The symmetric and antisymmetric stretching modes are represented by $R_s = ((R_1 + R_2)/2)$ and $R_a = R_1 - R_2$, respectively.

We next describe the numerical procedures for nuclear wave packet dynamics in one-dimensional space x. The total vibrational Hamiltonian $\hat{H}_x$ consists of the vibrational kinetic energy operator T_x for the two bond-stretching coordinates R_1 and R_2 and adiabatic potentials $V_x(R_1,R_2,t)$ in a laser field $\epsilon(t)$ obtained from eq 3. Calculation of the time evolution of a vibrational wave packet is carried out by using the split-operator for a small time increment Δt[47,48]

$$\psi(t+\Delta t) = \exp\left(-\frac{i\hat{H}_x \Delta t}{\hbar}\right)\psi(t) = \exp\left(-\frac{iV_x \Delta t}{2\hbar}\right) \exp\left(-\frac{i\hat{T}_x \Delta t}{\hbar}\right) \exp\left(-\frac{iV_x \Delta t}{2\hbar}\right)\psi(t) + O(\Delta t^3) \tag{10}$$

where t in $V_x(R_1,R_2,t)$ is replaced with the midpoint $t + (\Delta t/2)$. The operation of $\exp(-i\hat{T}_x \Delta t/\hbar)$ on a wave function is performed in momentum space by using fast Fourier transformation. A typical value of Δt used for the present simulation is 0.025−0.001 fs.

To cope with various temporal forms of the applied field, we fit a time-dependent adiabatic potential surface $V_x(R_1,R_2,t)$ to the following conventional form

$$V_x(R_1,R_2,t) = V_x(R_1,R_2,\epsilon{=}0) - \mu(R_1,R_2)\epsilon(t) - \frac{1}{2}\alpha(R_1,R_2)\epsilon^2(t) - \frac{1}{3}\beta(R_1,R_2)\epsilon^3(t) - \frac{1}{4}\gamma(R_1,R_2)\epsilon^4(t) \tag{11}$$

where $V_x(R_1,R_2,\epsilon{=}0)$ is the potential surface in a zero field. The functions μ, α, β, and γ of R_1 and R_2 are determined by fitting the form of $V_x(R_1,R_2,t)$ to the calculated potential surfaces at various static field strengths ϵ (up to $\epsilon = 0.2$ au).

B. Two-Dimensional Space. We next treat a case in which the molecule is placed on the x−y plane; i.e., $r_{1z} = r_{2z} = 0$. By making the following replacements in the x and y components in eq 7

$$q_{sx} = (r_{1x} + r_{2x})/2$$

$$q_{sy} = (r_{1y} - r_{2y})/2$$

$$q_{ax} = r_{1x} - r_{2x}$$

$$q_{ay} = r_{1y} + r_{2y}$$

we obtain

$$\hat{T} = -\frac{\hbar^2}{4m_O}\frac{\partial^2}{\partial {q_{sx}}^2} - \frac{M\hbar^2}{4m_C m_O}\frac{\partial^2}{\partial {q_{sy}}^2} - \frac{M\hbar^2}{m_C m_O}\frac{\partial^2}{\partial {q_{ax}}^2} - \frac{\hbar^2}{m_O}\frac{\partial^2}{\partial {q_{ay}}^2} \tag{12}$$

where $M = m_C + 2m_O$ is the total mass of the nuclei. The first two coordinates, q_{sx} and q_{sy}, can be divided into symmetric stretching and bending modes, and the last two coordinates, q_{ax} and q_{ay}, can be divided into two types of motion, namely, antisymmetric stretching and rotation. In the two-dimensional space model, we neglect q_{ax} and q_{ay} and set r_{1x} equal to r_{2x} and r_{1y} equal to $-r_{2y}$. The two C−O bond lengths, $R_1 = ({r_{1x}}^2 + {r_{1y}}^2)^{1/2}$ and $R_2 = ({r_{2x}}^2 + {r_{2y}}^2)^{1/2}$, are equal to each other: $R_1 = R_2 = R$. Using the following transformations

$$q_{sx} = R\cos\theta \quad \text{and} \quad q_{sy} = R\sin\theta \tag{13}$$

we obtain the kinetic energy for the symmetric stretching and bending modes

$$\hat{T}_{s-b} = -\frac{\hbar^2 M}{4m_O m_C}\left(\sin^2\theta\frac{\partial^2}{\partial R^2} - \frac{\sin 2\theta}{R^2}\frac{\partial}{\partial\theta} + \frac{\sin 2\theta}{R}\frac{\partial^2}{\partial R\partial\theta} + \frac{\cos^2\theta}{R}\frac{\partial}{\partial R} + \frac{\cos^2\theta}{R^2}\frac{\partial^2}{\partial\theta^2}\right) - \frac{\hbar^2}{4m_O}\left(\cos^2\theta\frac{\partial^2}{\partial R^2} + \frac{\sin 2\theta}{R^2}\frac{\partial}{\partial\theta} - \frac{\sin 2\theta}{R}\frac{\partial^2}{\partial R\partial\theta} + \frac{\sin^2\theta}{R}\frac{\partial}{\partial R} + \frac{\sin^2\theta}{R^2}\frac{\partial^2}{\partial\theta^2}\right) \tag{14}$$

where $\theta = \theta_1 = \theta_2$ is the angle between the x axis and a C−O bond axis, as shown in Figure 1. The bond bending angle in the conventional definition corresponds to $\pi - 2\theta$.

In the present two-dimensional model, the O−O axis is parallel to the polarization direction of $\epsilon(t)$ (x axis) and the adiabatic energy gives the same value for $\epsilon(t) = \pm|\epsilon(t)|$. The time-dependent adiabatic potential surface can therefore be fitted by the form

$$V_{s-b}(R,\theta,t) = V_{s-b}(R,\theta,\epsilon(t){=}0) - \frac{1}{2}\alpha(R,\theta)\epsilon^2(t) - \frac{1}{4}\gamma(R,\theta)\epsilon^4(t) \tag{15}$$

No odd order terms of $\epsilon(t)$ appear. (The permanent dipole vector points to the y direction.)

The split-operator method is not applicable to the operator $\hat{T}_{s-b}$ because the exponential form of $\hat{T}_{s-b}$ cannot be evaluated by Fourier transform. We here employ the Lanczos method,[48,49] which can be used for any form of the Hamiltonian operator. In this method, the total Hamiltonian at one time is diagonalized in terms of N_L basis functions generated by the Lanczos recursion scheme. (In this paper, $N_L \sim 7$.) Then an effective short-time propagator that is accurate up to Δt^{N_L-1} is constructed from the eigenvalues and eigenvectors.

4. Results and Discussion

The applied alternating electric field is assumed to have the form $\epsilon(t) = f(t)\sin\omega t$, where $f(t)$ is the field envelope. A

(46) Freed, K. F.; Lombardi, J. R. *J. Chem. Phys.* **1966**, *45*, 591−598.
(47) Feit, M. D.; Fleck, J. A., Jr. *J. Chem. Phys.* **1983**, *78*, 301−308. Kono, H.; Lin, S. H. *J. Chem. Phys.* **1986**, *84*, 1071−1079. Bandrauk, A. D.; Shen, H. *J. Chem. Phys.* **1993**, *99*, 1185−1193.
(48) Balakrishnan, N.; Kalyanaraman, C.; Sathyamurthy, N. *Phys. Rep.* **1997**, *280*, 79−144.
(49) Park, T. J.; Light, J. C. *J. Chem. Phys.* **1986**, *85*, 5870−5876. Leforestier, C. et al. *J. Comput. Phys.* **1991**, *94*, 59−80.

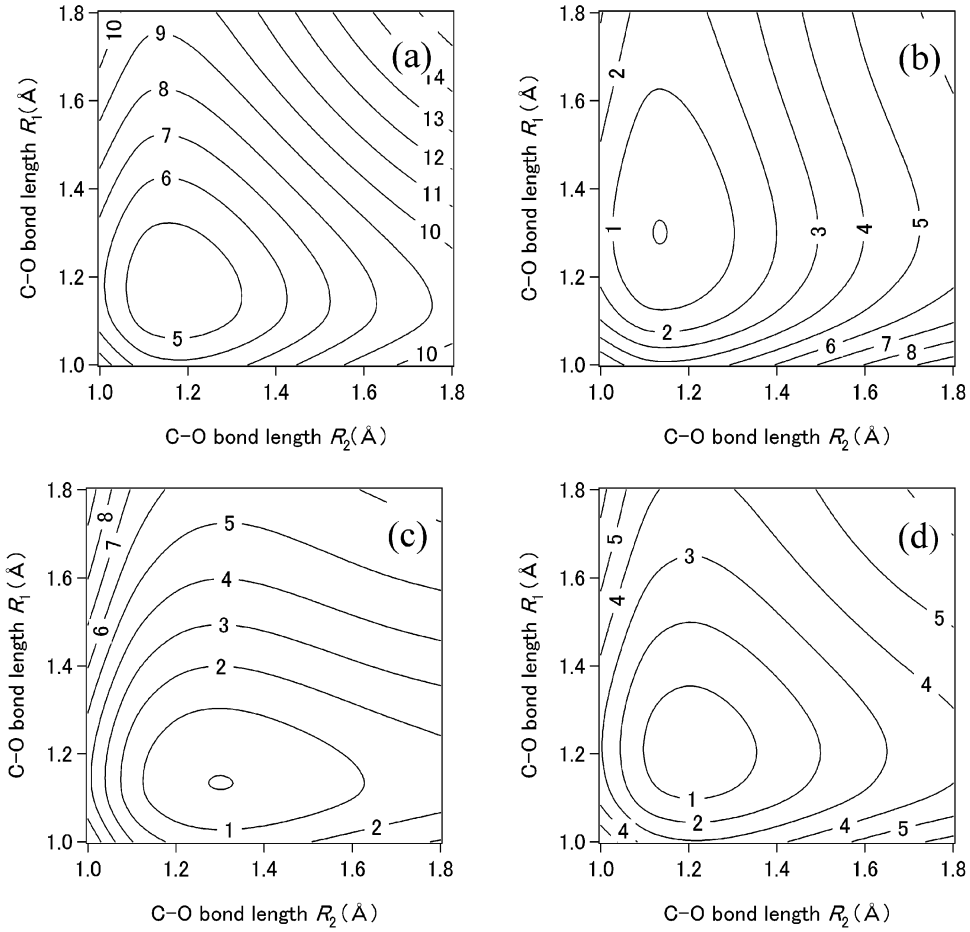

Figure 2. Potential surfaces of the lowest adiabatic state of CO_2 as a function of the two C−O bond distances R_1 and R_2. The contour lines are plotted at intervals of 1 eV. The field-free potential of the lowest state is shown in (a). The adiabatic potentials $V_x(R_1,R_2,t)$ at $\epsilon(t) = \pm$ (1/10) au are shown in (b) and (c), respectively. While the dissociation energy for a C−O bond is ∼7 eV in a zero field, it is greatly reduced, for instance, to 4 eV at a moment of $\epsilon(t) =$ (1/10) au as shown in (b). However, structural deformation such as one-bond stretching hardly occurs even at $f(t) \approx 2^{1/2}/10$ au. The nuclear dynamics is in fact governed by an effective potential, i.e., the average of $V_x(R_1,R_2,t)$ over one optical cycle, like the average of the adiabatic potentials at $\epsilon(t) = \pm$ (1/10) au shown in (d).

realistic pulse shape is employed

$$f(t) = f_0 \sin^2(\pi t/T_p) \quad \text{for} \quad 0 \le t \le T_p \tag{16}$$

and is otherwise zero. To reproduce the pulse used in the experiment, we choose the following parameters: peak strength $f_0 = 0.19$ au (1.3×10^{15} W/cm^2); pulse length $T_p = 194$ fs; and frequency $\omega = 0.057$ au ($\lambda = 795$ nm).

(i) Neutral CO_2 and CO_2^+. We first discuss the nuclear motion of neutral CO_2 in a field. For $\omega_{elec} \gg \omega$, where ω_{elec} represents the characteristic frequency for the electronic transitions, the present approach has the advantage that the electronic and vibrational motion is determined only by the lowest adiabatic state. In a zero field, the ground state is $^1\Sigma_g$ in the case of linear geometry and $^1A_1$ in the case of bent geometry under C_{2v} (for a symmetric stretching). The equilibrium structure is linear and the equilibrium internucler distance for a C−O bond, R_e, is 1.16 Å. (The calculated value is 1.17 Å.) To estimate how much electron density is transferred in a molecule, the total charge is assigned to each atom by Mulliken population analysis.[50] At $R_{C-O} = R_e$, the charges of O and C in a zero field are $-0.22e$ and $+0.45e$, respectively: the charge distribution of the main electronic configuration can be expressed as $O^{0+}C^{0+}O^{0+}$. From eq 6, $\epsilon_c = 0.05$ au at $R_{C-O} = R_e$. For the lowest adiabatic state at $\epsilon(t) = 0.1$ au $> \epsilon_c$, one of the O atoms is negatively charged as $-0.83e$. The ionic component $O^-C^{0+}O^+$ becomes dominant beyond ϵ_c. We thus expect for CO_2 that tunnel ionization via the ionic configuration predominantly occurs somewhere around ϵ_c. As expected, the calculated value of ϵ_c is larger than the intensity $I \approx 3 \times 10^{13}$ W cm^{-2} ($f(t) \approx$ 0.03 au) at which CO_2^+ appears experimentally.[44]

We have calculated the potential surface of the lowest adiabatic state of CO_2 as a function of the two C−O bond distances R_1 and R_2 and the bond angle 2θ. Bond stretching can be classified into two types: symmetric two-bond stretching, in which $R_1 = R_2$, and one-bond stretching, in which one C−O bond is longer than the other (e.g., $R_1 > R_2 = R_e$). The field-free potential of the lowest state of CO_2 in the case of linear geometry, $V_{x,1}(R_1,R_2,\epsilon=0)$, is shown in Figure 2a. The adiabatic potential $V_{x,1}(R_1,R_2,t)$ is greatly distorted in an intense field; the dissociation energy for a C−O bond is ∼7 eV in a zero field and is reduced to 4 eV at a moment of $\epsilon(t) = (1/10)$ a.u. ($>\epsilon_c$), as shown in Figure 2b. However, structural deformation such as one-bond stretching hardly occurs even at $f(t) \approx 2^{1/2}/10$ au as explained below.

(50) Levin, I. R. *Quantum Chemistry*, Prentice Hall: Englewood Cliffs, NJ, 2000; pp 505−508.

The key is the fact that when the sign of the field is reversed, the dissociation energy for the C−O bond under consideration increases, as shown in Figure 2c. The second term $-\mu(R_1,R_2)\epsilon(t)$ in the lowest adiabatic potential $V_{x,1}(R_1,R_2,t)$ expanded as in eq 11 can be approximated as $-R_a g(R_s)\epsilon(t)$, where $g(R_s)$ is a function of the symmetric stretching coordinate. Since $-\mu(R_1,R_2)$ is more or less proportional to the antisymmetric coordinate R_a, the barrier for one of the one-bond dissociation (two-body breakup) channels O + CO and OC + O is greatly reduced when $|\epsilon(t)|$ is large, as mentioned above. It should, however, be noted that the following inequality in temporal or energy scale holds

$$\omega_{elec} > \omega > \omega_{vib} > \dot{f}(t)/f(t) \sim 1/T_p \qquad (17)$$

where ω_{vib} is the vibrational frequency. The experimental condition $\omega \gg \omega_{vib}$ means that the change in $\epsilon(t)$ is too fast for the vibrational motion to follow the change in $\epsilon(t)$ adiabatically. Moreover, $\omega \gg \dot{f}(t)/f(t)$ means that $f(t)$ does not change in one optical cycle ($2\pi/\omega$) (which is much shorter than the pulse length T_p). The nuclear dynamics is thus expected to be governed by an effective potential like the average of the adiabatic potentials at $\epsilon(t) = \pm$ (1/10) au shown in Figure 2d.

The precise effective potential can be given by replacing $\epsilon^j(t)$ in $V_x(R_1,R_2,t)$ with the average $(\omega/2\pi)\int_{t-\pi/\omega}^{t+\pi/\omega} \epsilon^j(t')\,dt'$ over one optical cycle (where $j = 1, 2, ...$)

$$\bar{V}_x(R_1,R_2,t) = V_x(R_1,R_2,\epsilon{=}0) - \frac{1}{4}\alpha(R_1,R_2)f^2(t) - \frac{3}{32}\gamma(R_1,R_2)f^4(t) \qquad (18)$$

In the cycle-averaged potential $\bar{V}_x(R_1,R_2,t)$, the odd order terms of $\epsilon(t)$, such as the dipole interaction term, disappear. Therefore, the actual dynamics is governed by the pulse amplitude $f(t)$. The leading perturbation term in $\bar{V}_x(R_1,R_2,t)$ is given by the polarization energy proportional to α. The polarizability α has a ridge along the line $R_1 = R_2$: the dissociation energy in $\bar{V}_x(R_1,R_2,t)$ for the symmetric stretching mode is greatly reduced from 15.5 to 7 eV as $f(t)$ increases from 0 to $f(t) \approx 2^{1/2}/10$ au ($\gg\epsilon_c$). Figure 2d is almost identical to $\bar{V}_x(R_1,R_2,t)$ at $f(t) = 2^{1/2}/10$ au ($\sim 7 \times 10^{14}$ W cm^{-2}). However, a comparison of parts a and d of Figure 2 shows that the equilibrium geometry in $\bar{V}_x(R_1,R_2,t)$ is, up to $f(t) \approx 2^{1/2}/10$ au, almost equal to that in a zero field. The equilibrium internuclear C−O distance is calculated to be 1.19 Å at $f(t) \approx 2^{1/2}/10$ au. Since $\omega_{vib} > \dot{f}(t)/f(t)$, the vth vibrational state in a zero field is adiabatically transferred to the vth state of $\bar{V}_x(R_1,R_2,t)$. Bond stretching scarcely occurs, and the width of the wave function hardly increases. Bending motion is not induced for $f(t) \leq 2^{1/2}/10$ au, either: at a fixed internuclear distance, the curvature of the potential along θ increases as $|\epsilon(t)|$ increases.

We thus conclude that CO_2 maintains its stable linear structure around $R_e \approx 1.17$ Å even at field strengths $f(t) \approx 2^{1/2}/10$ au. In the neutral stage, ionization begins at $f(t) \approx 0.03$ au before the field intensity becomes high enough to deform the molecule. In the case of small R, the energy difference between the first excited and ground electronic states is much larger than ω: only the lowest adiabatic state is populated, as we have assumed. In the CO_2^+ stage, ionization occurs before the field intensity becomes high enough to deform the molecule, as in CO_2.

(ii) CO_2^{2+} Molecule. The geometry of CO_2^{2+} just after ionization of CO_2^+ is expected to be more or less equal to the equilibrium geometry of CO_2 . The vibrational wave function of the initially prepared state of CO_2^{2+} can be expressed by the product of the wave function of the ground vibrational state of CO_2 and the ionization rates of CO_2 and CO_2^+ as functions of nuclear coordinates. Since the explicit forms of the ionization rates are unknown, we test two extreme cases. The first one is the vertical transition case in which the initial vibrational state of CO_2^{2+} is the ground vibrational state of CO_2. The second one is the adiabatic transition case in which CO_2^{2+} starts from its ground vibrational state. Considering that the ionization probability generally has a peak around an internuclear distance larger than the equilibrium internuclear distance, the peak of the initial vibrational wave function of CO_2^{2+} is presumably expressed by shifting the wave function of the ground vibrational state of CO_2 toward larger internuclear distances. Since the equilibrium internuclear distance of CO_2^{2+} (the calculated value being 1.22 Å) is longer than 1.17 Å of CO_2, the actual situation will be a little shifted from the vertical transition case toward the adiabatic transition case.

In the stage of CO_2^{2+}, consideration must be given to at least the lowest three adiabatic states of CO_2^{2+}, the ground triplet state connected with the $^3B_1$ state ($^3\Sigma_g$ in the case of linear geometry) in a zero field and the nearly degenerate lowest singlet states connected with $^1A_1$ and $^1B_1$ in a zero field ($^1\Delta_g$ in the case of linear geometry). The energy difference between $^1A_1$ and $^3B_1$ in a zero field is as small as ∼1.5 eV near the equilibrium geometry of $R_e \approx 1.2$ Å. When CO_2^+ is ionized, the laser field strength is higher than $I \approx 5 \times 10^{13}$ W cm^{-2}.[51] Therefore, the difference of ∼1.5 eV (∼one photon energy) may not be decisive in the preparation of CO_2^{2+}; there is a possibility that the lowest three states are almost equally populated. Fortunately, the potential surfaces of the lowest three adiabatic states have nearly the same shape in a wide range of field strengths.[28]

Results of Mulliken population analysis show nearly the same atomic charge distributions for the lowest three adiabatic states of CO_2^{2+} in a field. Therefore, for the three adiabatic states, almost the same net charges are expected to be transferred among nuclei by a field. Since Coulomb explosions of $O^+ + C^+ + O^+$ are experimentally observed more or less at $I \geq 3 \times 10^{14}$ W cm^{-2},[51] the small differences in the ionization potential between the lowest three adiabatic states of CO_2^{2+} will make only a small difference in the ionization rate. Therefore, the electronic and nuclear dynamics in the CO_2^{2+} stage is nearly the same irrespective of which state is prepared among the lowest three adiabatic states.

In the three adiabatic states, two positive charges are nearly equally distributed among the three atoms. We assume that the state consists of three main configurations, OC^+O^+, O^+C^+O, and O^+CO^+. The ionic configuration favorable for tunnel ionization is $O^-C^+O^{2+}$, created from OC^+O^+. The field strength required for this crossing as estimated by eq 6 is $\epsilon_c = 0.18$ au in the case of the equilibrium geometry $R_1 = R_2 = R_e$. As will be shown below, structural deformation of CO_2^{2+} can occur before the field strength reaches the large threshold value of 0.18 au, i.e., before ionization. As a representative case, we present results of calculation of nuclear wave packet dynamics

(51) Hishikawa, A.; Yamanouchi, K. Private communication.

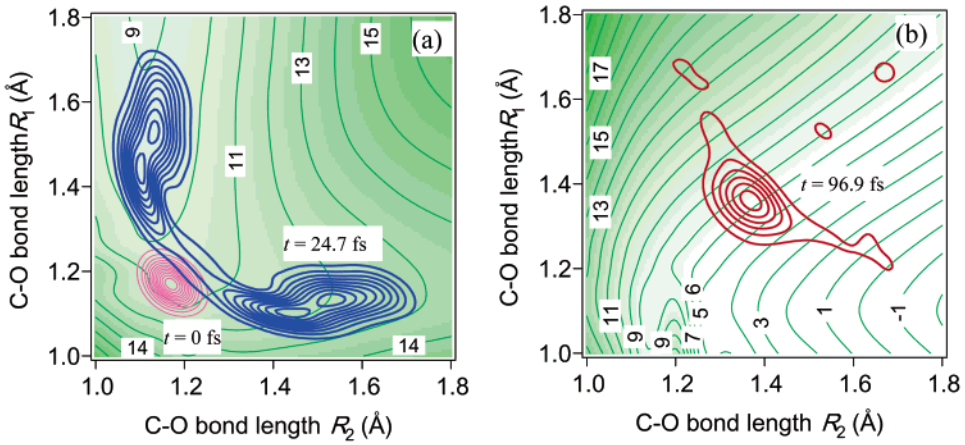

Figure 3. Nuclear wave packet dynamics in the lowest adiabatic state $|1\rangle$ of CO_2^{2+} in the vertical transition case. The applied field is given by eq 16: peak strength $f_0 = 0.19$ au (1.3×10^{15} W/cm^2), pulse length $T_p = 194$ fs, and wavelength $\lambda = 795$ nm. We here assume vertical transition from CO_2 for which the wave function prepared at $t = 0$ in $|1\rangle$ is that of the ground vibrational state of CO_2. The squares of the nuclear wave functions at $t = 0$ and $t = 24.7$ fs are denoted by the pink and blue contour lines in (a), respectively; the wave packet at $t = 96.9$ fs (red lines) is shown in (b). The instantaneous adiabatic potentials of $|1\rangle$ at $\epsilon(t = 24.7\text{ fs}) = -0.029$ au and $\epsilon(t = 96.9\text{ fs}) = 0.19$ au (both are local extrema of the field) are shown in (a) and (b), respectively; the green contour lines are plotted at intervals of 1 eV. As shown in (b), although the adiabatic potential can be dissociative at a moment for one of the two-body breakup channels, one-bond stretching is not greatly enhanced by the field.

starting from the lowest adiabatic state of CO_2^{2+} adiabatically connected to $^3B_1$. The parameters of the applied pulse are given in eq 16.

A. Simultaneous Two-Bond Stretching: A Characteristic of Dynamics in Intense Fields. We examine the nuclear dynamics in the lowest adiabatic state potential $V_{x,1}(R_1,R_2,t)$ as a function of the two bond-stretching coordinates R_1 and R_2 (linear geometry case). The dissociation energy in a zero field is ~11 eV in the case of symmetric two-bond stretching (5 eV smaller than that of CO_2) and ca. 1 eV in the case of one-bond stretching. From the viewpoint of dissociation energy, it is expected that one-bond stretching is predominant. As will be shown below, however, the wave packet dynamics shows that symmetric stretching occurs as well as one-bond stretching.

Vertical Transition from the Ground Vibrational State of CO_2. We assume that the wave function of the ground vibrational state of CO_2 is prepared at $t = 0$ in the lowest adiabatic state of CO_2^{2+}. In Figure 3a, the square of the initial wave function is denoted by the pink contour circles around $R_1 = R_2 \approx 1.2$ Å. As shown by the wave packet at $t = 24.7$ fs in Figure 3a, a part of the wave packet propagates first toward the channels for one-bond stretching from the Franck−Condon region. The instantaneous potential at $\epsilon(t = 24.7\text{ fs}) = -0.029$ au is denoted by green contour lines. Around $t = 45$ fs, the main part of the wave packet returns to the vicinity of $R = 1.2$ Å. The initial one-bond stretching is not an effect of the applied field; it originates from the difference in the equilibrium internuclear distance between CO_2^{2+} and CO_2. This is confirmed by the fact that the initial one-bond stretching is reproduced in a zero field.

We propose that the experimentally observed two-body breakup to $CO^+ + O^+$ is due to the one-bond stretching in the adiabatic potential of CO_2^{2+}. To estimate the probability of occurrence of one-bond dissociation, a detection window with a width of $R_2 = (0, 1.2$ Å) is set at $R_1 = 1.7$ Å, and a window of the same width is set for the other bond. In a zero field, all of the dissociation components are detected by the two windows; the probability for one-bond dissociation channels is $P_{one} \sim 0.14$. In the presence of the field, the probability detected by these windows is $P_{one} \sim 0.20$. Subsequent ionization processes are not taken into account here. The adiabatic potential can be dissociative at a moment for one of the two-body breakup channels, as shown by the instantaneous potential at $\epsilon(t = 96.9$ fs$) = 0.19$ au in Figure 3b. However, considering that the total dissociation probability is ~0.70, one-bond stretching is not greatly enhanced by the field, as indicated by the wave packet at $\epsilon(t = 96.9$ fs$) = 0.19$ au in Figure 3b. This is due to the disappearance of the odd order terms with $\epsilon(t)$ in the cycle-averaged potential $\bar{V}_{x,1}(R_1,R_2,t)$ of CO_2^{2+}, as in the case of CO_2. The dynamics of the wave packet in the cycle-averaged potential is identical with the "raw" dynamics shown in Figure 3.

Although the dissociation energy in a zero field is ~11 eV in the case of symmetric stretching, symmetric two-bond stretching becomes dominant as the field envelope approaches $f(t \approx 50$ fs$) = 0.1$ au ($I \approx 3.5 \times 10^{14}$ W cm^{-2}); the center of the wave packet moves to a region of $R_1 = R_2$ (=1.4 Å at $t =$ 96.9 fs, as shown in Figure 3b). The appearance of field-induced symmetric two-bond stretching can be explained by the characteristic features of $\bar{V}_{x,1}(R_1,R_2,t)$. The cycle-averaged potentials at $t = 24.7$ fs and $t = 96.9$ fs are shown in Figure 4. In CO_2^{2+}, the stabilization energy $-\alpha(R_1,R_2)f(t)^2/4$ due to the induced dipole moment is large around the ridge of $R_1 = R_2$ relative to the field-free dissociation energy for symmetric stretching. Consequently, the steepest descending slope from $R_1 = R_2 = R_e$ is formed at high intensities along $R_1 = R_2$ in $\bar{V}_{x,1}(R_1,R_2,t)$, as shown in Figure 4b. The dissociation energy for the symmetric coordinate in $\bar{V}_{x,1}(R_1,R_2,t)$ is just 2.2 eV at $f(t) = 2^{1/2}/10$ au; at higher field intensities, the symmetric stretching becomes unbound. The difference between the total dissociation probability and the one-bond dissociation probability, P_{one}, can be used as the probability of occurrence of field-induced symmetric two-bond dissociation, $P_{sym}(\approx 0.50)$.

After bond stretching, CO_2^{2+} is ionized due to enhanced ionization at larger values of $R > R_e$. It should be noted that the value of ϵ_c decreases with increases in R. For instance, $\epsilon_c = 0.14$ au at $R = 1.4$ Å. Moreover, as R increases, in the ionic configuration $O^-C^+O^{2+}$, the attractive force due to the distant nuclei O^{2+} and C^+ against electrons in O^- becomes weaker.

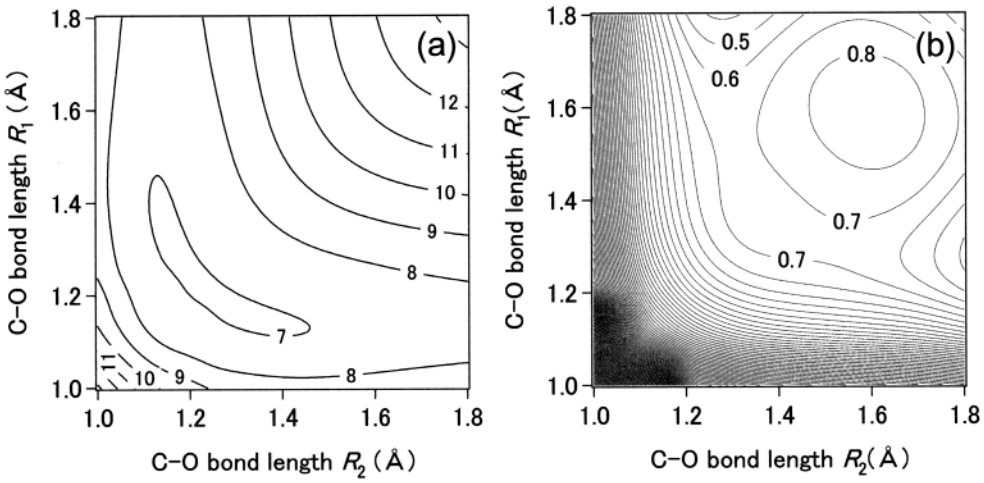

Figure 4. Cycle averages of the lowest adiabatic potential $V_{x,1}(R_1,R_2,t)$ of CO_2^{2+} at (a) $t = 24.7$ fs and (b) $t = 96.9$ fs. The cycle-averaged potential is obtained by averaging $V_{x,1}(R_1,R_2,t)$ over one optical cycle. The intervals between contour lines for (a) and (b) are 1 and 0.1 eV, respectively. As shown in (a), around $f(t = 24.7 \text{ fs}) \approx 0.029$ au, the dissociation energy for symmetric two-bond stretching is as large as the field-free dissociation energy (~11 eV). As the field intensity increases, the stabilization energy due to the induced dipole moment becomes large: the steepest descending slope from $R_1 = R_2 = 1.2$ Å is formed along $R_1 = R_2$, as shown in (b). The cycle-averaged potential is symmetric with exchange of R_1 and R_2 because of the disappearance of the odd order terms with $\epsilon(t)$.

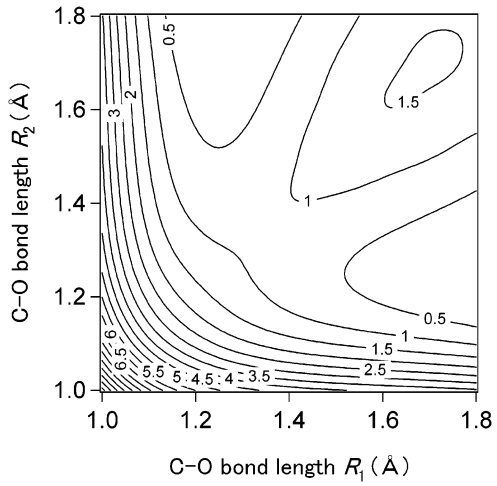

Figure 5. Potential of the field-free lowest adiabatic potential of CO_2^{3+}. The heights of contour lines are indicated in units of eV. The potential surface has a saddle point around $R_1 = R_2 = R = 1.35$ Å, from which a hill gently ascends to a peak around $R = 1.7$ Å by a height of 0.5 eV. In the region of $R > 1.7$ Å, the potential of CO_2^{3+} decreases as $5/2R$ owing to the dominant Coulomb repulsions of the three positively charged atoms.

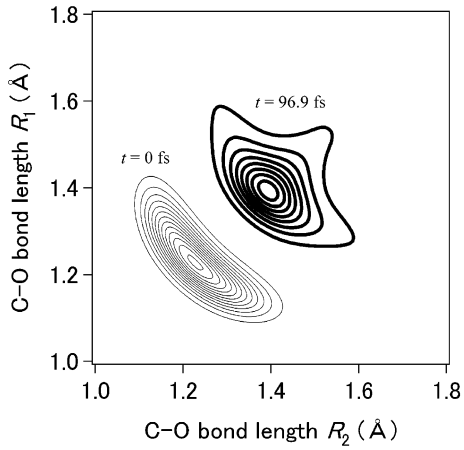

Figure 6. Nuclear wave packet dynamics in the lowest adiabatic state $|1\rangle$ of CO_2^{2+} in the adiabatic transition case. The wave packet starts from the ground vibrational state in $|1\rangle$. The two contour maps denote snapshots of the nuclear wave packets at $t = 0$ fs (solid contour lines) and 96.9 fs (bold contour lines). As the field intensity increases, the center of the wave packet moves along the line $R_1 = R_2$ of symmetric stretching.

Once an ionic component of $O^-C^+O^{2+}$ is created at large R as the field intensity approaches ϵ_c, ionization therefore occurs at a high probability. Hence, after bond stretching in CO_2^{2+}, ionization to CO_2^{3+} occurs even at field strengths that do not ionize CO_2^{2+} around R_e (enhanced ionization).

As shown in Figure 5, the potential surface of the field-free lowest adiabatic state ($^2\Pi$ in the case of linear geometry) of CO_2^{3+} has a saddle point around $R_1 = R_2 = 1.35$ Å, from which a hill gently ascends to a peak around $R_1 = R_2 = 1.7$ Å by a height of 0.5 eV. In the region of $R_1 = R_2 > 1.7$ Å, the potential of CO_2^{3+} governed by the Coulomb repulsions of the three atoms decreases as $5/2R_s$. If ionization to CO_2^{3+} occurs, say, around $R_1 = R_2 = 1.7$ Å, the nuclear wave packet is then at the top of the hill of CO_2^{3+}: the CO_2^{3+} created will undergo Coulomb explosions to $O^+ + C^+ + O^+$.

When CO_2^+ is ionized, the intensity is not high enough to deform the potential. Therefore, the subsequent wave packet dynamics of CO_2^{2+} is not affected by starting the wave packet of CO_2^{2+} at the moment when CO_2^+ is ionized, e.g., at $t_c \approx 33$ fs for which $f(t_c) = \epsilon_c = 0.05$ au is satisfied. The wave packet prepared at $t = t_c$ first undergoes one-bond stretching and then meanders in the vicinity of $R = 1.2$ Å until two-bond stretching begins, as in the case of starting at $t = 0$.

Adiabatic Transition to CO_2^{2+}. In the adiabatic transition case, the initial wave packet is the ground vibrational state in the lowest adiabatic state of CO_2^{2+}. The wave packet dynamics under the condition of the same pulse as that used before is illustrated in Figure 6. The probability of going through the detection windows for one-bond stretching, P_{one}, is ~0.13. This value is smaller than that in the vertical transition case. In the adiabatic transition case, one-bond stretching is purely field-induced; initial one-bond stretching as observed in the vertical transition case does not occur. The total dissociation probability is 0.48, and the probability of field-induced two-bond dissociation, P_{sym}, is 0.35. The ratio P_{sym}/P_{one} is only a little larger in

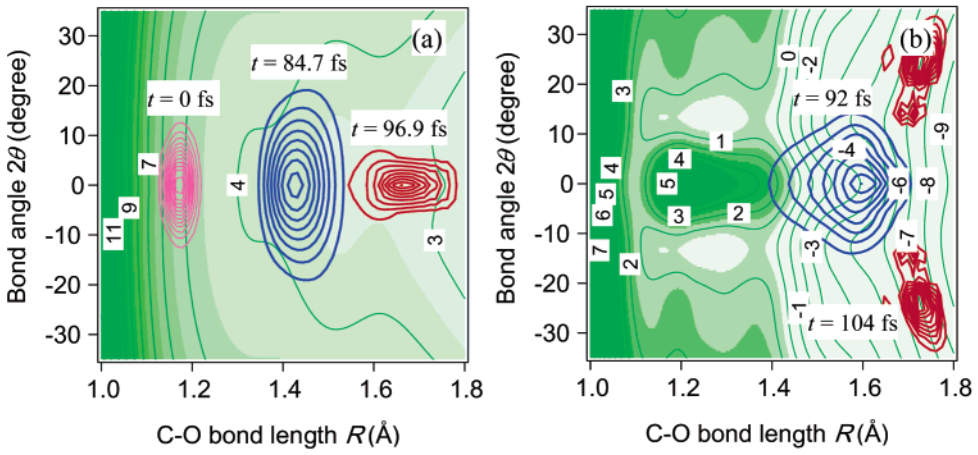

Figure 7. Wave packet propagation on (a) the lowest adiabatic state $|1\rangle$ and (b) the second lowest adiabatic state $|2\rangle$ of CO_2^{2+} in the vertical transition case. The contour maps denoted by green lines (plotted at intervals in 1 eV) are the cycle-averaged potentials of (a) $|1\rangle$ at $t = 84.7$ fs and (b) $|2\rangle$ $t = 92$ fs. In (a), snapshots of the wave packet are taken at $t = 0$ (pink contour lines), $t = 84.7$ fs (blue lines), and $t = 96.9$ fs (red lines). In (b), snapshots of the wave packet are taken at $t = 92$ fs (blue lines) and $t = 104$ fs (red lines). We have assumed that a nonadiabatic transition from $|1\rangle$ to $|2\rangle$ occurs only once at $t \approx 92$ fs. (The population of $|2\rangle$ is normalized at this moment.) In the initial stage up to ~70 fs, the mean amplitude of bending, $\langle(2\theta)^2\rangle$, is doubled at most (~12°). However, the curvature of the cycle-averaged potential with θ is large at large R: as shown in (a), after the wave packet passes a point of ~1.6 Å, the amplitude of bending motion in $|1\rangle$ decreases. On the other hand, as shown in (b), the cycle-averaged potential of $|2\rangle$ has two minima at $2\theta \approx 15°$. Consequently, the component in $|2\rangle$ nonadiabatically transferred from $|1\rangle$ is split into two parts toward large bending angles.

the adiabatic transition case than in the vertical transition case where one-bond stretching initially occurs. In an alternating field whose frequency is larger than the vibrational frequencies, symmetric two-bond stretching is generally more field induced than is one-bond stretching.

B. Correlation between Bond Angle Bending and Symmetric Stretching: Importance of Field-Induced Nonadiabatic Transition. We now clarify the origin of the experimentally observed bending amplitude, $\langle(2\theta)^2\rangle \approx 20°$, of exploding CO_2^{3+}.[11] We show that this large amplitude results from a strong correlation between the bending and stretching modes through field-induced nonadiabatic transitions. The calculated bending frequency of CO_2^{2+} in a zero field is $^6/_{10}$ths as large as that of CO_2; if the initially prepared state is the ground vibrational state of CO_2^{2+} (adiabatic transition case), the mean amplitude of the bending motion, $\langle(2\theta)^2\rangle$, increases only $1/0.6^{1/2} \approx 1.3$ times on going from CO_2 to CO_2^{2+}. In the vertical transition case, the wave packet initially prepared from CO_2 is a linear combination of the ground and *excited* vibrational states of the bending mode in the lowest adiabatic state of CO_2^{2+}. Since the curvature of the potential with θ is smaller in CO_2^{2+} than in CO_2, the initially prepared wave packet spreads out along θ. When the pulse is off, the maximum of the mean amplitude for bond angle bending 2θ is ~9°, which is one and one-half times larger than the initial value (~6°). The mean amplitude of ~9° is still smaller than the experimentally observed value, ~20°. The experimentally observed large-amplitude bending motion cannot be attributed to the structural change between CO_2 and CO_2^{2+} in a zero field.

The energy shift due to the induced dipole is nearly proportional to $-R_s \cos\theta$ because field-induced charge separation occurs between the two O atoms. The induced dipole of the lowest adiabatic state that shifts the energy downward becomes smaller as the molecule becomes more bent; as a result, the curvature of the potential with θ is larger in a nonzero field than in a zero field. Therefore, if the internuclear distances are fixed, a large-amplitude bending motion is hardly induced by a field. To examine how the bending motion is correlated with bond stretching, we here focus on the role of the symmetric stretching characteristic of intense-field dynamics; the two-dimensional Hamiltonian constructed from the bending and symmetric stretching modes is used.

The wave packet propagation on the lowest adiabatic state $|1\rangle$ of CO_2^{2+} is shown together with the cycle-averaged potential at $t = 84.7$ fs in Figure 7a. We assumed the vertical transition case. In the initial stage up to ~70 fs, at periodic intervals of 30−35 fs, the wave packet moves back and forth along the symmetric stretching coordinate R (between $R = 1.2$ and $R = 1.4$ Å) and repeatedly spreads and shrinks in the bond angle direction. The quasiperiodic motion originates from the fact that the potential surface of CO_2^{2+} is shallower than that of CO_2. The cycle-averaged potential of $|1\rangle$ is rather flat with respect to the change in the bond angle 2θ for $R < 1.5$ Å. The bending amplitude is doubled at most (~12°), as shown by the wave packet at $t = 84.7$ fs in Figure 7a. However, the curvature of the cycle-averaged potential with θ is large at large R: as shown by the wave packet at $t = 96.9$ fs (the peak of the pulse) in Figure 7a, after the wave packet passes a point of ~1.6 Å, the amplitude of bending motion in $|1\rangle$ decreases. The dynamics in $|1\rangle$ alone is not sufficient to explain the experimentally observed large-amplitude bending.

In the following, we show that field-induced nonadiabatic transition between the lowest two adiabatic states, $|1\rangle$ and $|2\rangle$, is essential for describing the experimentally observed large-amplitude bending. As shown in Figure 8, the difference in energy between the lowest two adiabatic states in a zero field becomes smaller than one photon energy 0.057 au (1.55 eV) in the large bond length region ($R > 1.7$ Å). The difference also decreases as the bending angle increases because the second lowest adiabatic state in a zero field has double minima at $2\theta = \pm 12°$ due to the Renner−Teller effect;[52] the first excited triplet state is a degenerate $^3\Delta$ of the main configuration (next HOMO $1\pi_u)^3$ (HOMO $1\pi_g)^3$ in the case of linear geometry. It is thus expected that the nonadiabatic transition between the

(52) Herzberg, G. *The spectra and structures of simple free radicals, An introduction to Molecular spectroscopy*; Cornell University Press: Ithaca, NY, 1971.

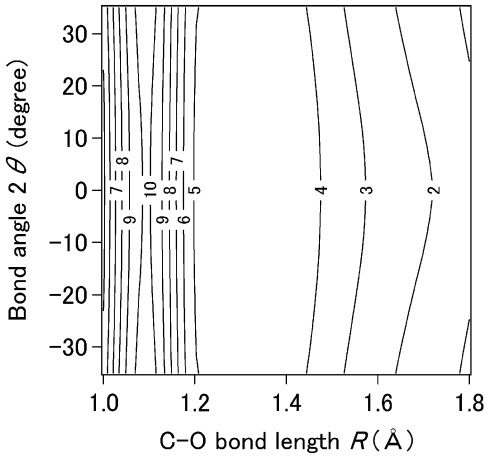

Figure 8. Difference in energy between the lowest two field-free adiabatic states of CO_2^{2+} as a function of the bending angle 2θ and symmetric stretching coordinate R (C−O bond length). The contour map is plotted in units of eV. The difference becomes smaller than one photon energy 0.057 au (1.55 eV) at large internuclear distances ($R > 1.7$ Å). The difference also decreases as 2θ increases.

lowest two states is strongly correlated with the bending or stretching motion. It is known that the Renner−Teller interaction induces various dynamical effects[53] as well as spectroscopic perturbations.

The energy gap between the lowest two states $|1\rangle$ and $|2\rangle$ of CO_2^{2+} is 2−3 eV (∼0.1 au) around the point where $R = 1.6$ Å and the bending angle $2\theta = 10°$. In the case of this structure, the nonadiabatic transition probability estimated by the Landau−Zener formula of eq 5 takes a maximum value of about 0.11, e.g., at $t \approx 91.6$ fs. At this moment, $\epsilon(t) = 0.15$ au and $f(t) \approx 0.19$; from the MCSCF calculation, $E_2(t) - E_1(t) \approx 0.07$ au and $\mu_{12}(t) \approx 0.27$ au. Since $E_2(t) - E_1(t)$ decreases rapidly with increases in R, we expect that nonadiabatic transitions predominantly take place at internuclear distances larger than ∼1.6 Å. In the present simulation, we simply assume that a nonadiabatic transition from $|1\rangle$ to $|2\rangle$ occurs only once at $t \approx 92$ fs. At this moment, the center of the wave packet is located around $R = 1.6$ Å, as shown by the wave packet at $t = 92$ fs in Figure 7b. The subsequent nonadiabatic transitions are ignored. Around $R \approx 1.4-1.7$ Å, the cycle-averaged potential of $|2\rangle$ at $t = 92$ fs shown in Figure 7b has two minima in the bond angle direction, which reflects the double-minimum structure of the zero-field potential. Consequently, the component in $|2\rangle$ nonadiabatically transferred from $|1\rangle$ is split into two parts toward large bending angles, as shown by the wave packet at $t = 104$ fs in Figure 7b: the mean amplitude of bending motion in $|2\rangle$ is as large as the experimental value of ∼20° at $R \approx 1.7$ Å. The same conclusion is drawn in the adiabatic transition case. The role of nonadiabatic transitions is crucial for bending, while the average bond distance depends only weakly on whether the wave packet propagates on $|1\rangle$ or $|2\rangle$.

The nonadiabatic transition probability increases as the molecule becomes bent. Bent molecules preferentially transferred to $|2\rangle$ from $|1\rangle$ are then further bent. Since more charge is transferred in $|2\rangle$ than in $|1\rangle$, the ionization probability of $|2\rangle$ is expected to be larger than that of $|1\rangle$. Thus, the wave packet in the upper adiabatic state probably makes a larger contribution to the experimentally observed Coulomb explosion channel of $O^+ + C^+ + O^+$. We presume that the bent configuration of an exploding $O^+ + C^+ + O^+$ is the structure of CO_2^{2+} just before the Coulomb explosion.

Since the structural deformation is determined by the shape of the cycle-averaged potential, the molecular dynamics in a field perpendicular to the molecular axis is dominated by the perpendicular component of the polarizability, α_{yy}. For CO_2 and its cations, α_{yy} increases by ∼1 au as the bending angle 2θ changes from 0° to 20°. Although the increase in α_{yy} is small, a perpendicular field may slightly increase the bending amplitude because the curvature along θ is small. However, a perpendicular field does not sufficiently reduce the large dissociation energy to induce bond stretching (as the bond length R increases from 1.2 to 1.6 au, α_{yy} increases by only 3 au). We thus conclude that the perpendicular configuration is not responsible for the experimentally observed bond stretching accompanied by a large amplitude motion.

5. Control of Two-Bond Dissociation

We have shown that the fate of the molecular dynamics in an intense laser field is determined by the cycle-averaged potential. It is therefore possible to control the molecular dynamics in intense fields by modifying the cycle-averaged potential. One of the most commonly used schemes is the combination of ω and 2ω fields[54]

$$\epsilon(t) = F(t)[\sin \omega t + \eta \sin(2\omega t + \phi)] \tag{19}$$

where ϕ and η are the relative phase and amplitude between the ω and 2ω fields, respectively, and $F(t)$ is the slowly varying field amplitude. While $\langle\epsilon(t)\rangle$ over a period of $2\pi/\omega$ is zero as in the single ω-frequency case, the cycle-average of $\epsilon^3(t)$ is nonzero except in the case of $\phi = 0$

$$\langle\epsilon^3(t)\rangle = F^3(t)\langle[\sin \omega t + \eta \sin(2\omega t + \phi)]^3\rangle = -3\eta(\sin \phi)F^3(t)/4 \tag{20}$$

To assess the effect of the nonzero cycle average of $\epsilon^3(t)$ judiciously, we set $\langle\epsilon^2(t)\rangle$ equal to that in the single ω-frequency case. By choosing the field amplitude as

$$F(t) = f(t)/(1 + \eta^2)^{1/2} \tag{21}$$

we have the same $\langle\epsilon^2(t)\rangle$ as that in the single ω-frequency case: $\langle\epsilon^2(t)\rangle = (1 + \eta^2)(F^2(t)/2) = (f^2(t)/2)$. Thus, the difference in dynamics between the single and double frequency cases can be attributed mainly to the nonzero $\langle\epsilon^3(t)\rangle$. The final form of $\langle\epsilon^3(t)\rangle$ becomes

$$\langle\epsilon^3(t)\rangle = -3\eta(\sin \phi)f^3(t)/4(1 + \eta^2)^{3/2} \tag{22}$$

We consider the case in which $\langle\epsilon^3(t)\rangle$ is maximized: $\eta = 1/2^{1/2}$ and $\phi = \pm(\pi/2)$. The amplitude $f(t)$ and the fundamental frequency ω are the same as those used in eq 16. In the vertical $CO_2 \rightarrow CO_2^{2+}$ transition case, the dissociation probability for one-bond stretching channels is $P_{one} \sim 0.39$, while the prob-

(53) Fujimura, Y.; Hayashi, H.; Nagakura, S. *Chem. Phys.* **1992**, *162*, 205−212.

(54) Charron, E.; Giusti-Suzor, A.; Mies, F. H. *Phys. Rev. A* **1994**, *49*, R641−644. Kanai, T.; Sakai, H. *J. Chem. Phys.* **2001**, *115*, 5492−5497. Baranova, N. B.; Reiss, H. R.; Zel'dovich, B. Ya. *Phys. Rev. A* **1993**, *48*, 1497−1505. Sheehy, A.; Walker, B.; Di Mauro, L. F. *Phys. Rev. Lett.* **1995**, *74*, 4799−4802. Bandrauk, A. D.; Levesque, J.; Chelkowski, S. In ref 2, pp 221−235.

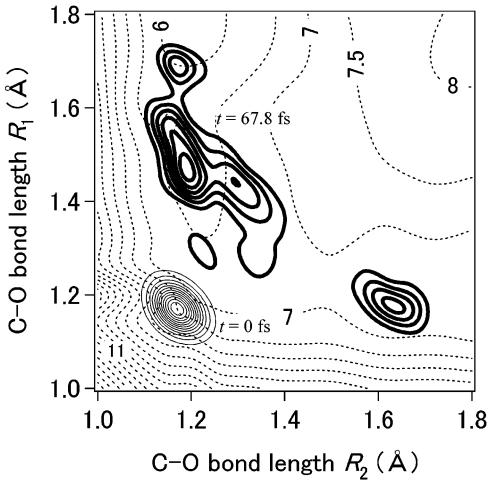

Figure 9. Nuclear wave packet dynamics in the lowest adiabatic state of CO_2^{2+} in a $\omega + 2\omega$ field $\epsilon(t) = f(t)[\sin \omega t + \eta \sin(2\omega t + \phi)]/(1 + \eta^2)^{1/2}$. The relative phase and amplitude between the ω and 2ω fields are chosen so that the nonzero cycle average of $\epsilon^3(t)$ is maximized: $\phi = (\pi/2)$ and $\eta = 1/2^{1/2}$. We assume that the initial nuclear wave packet at $t = 0$ (solid contour lines) around $R_e \approx 1.2$ Å is prepared by the vertical transition from CO_2. The contour map denoted by bold solid lines shows the wave packet at $t = 67.8$ fs. The cycle-averaged potential of the lowest adiabatic state at $t = 67.8$ fs is denoted by dotted contour lines (in units of eV). The combination of the intense ω and 2ω fields induces asymmetric one-bond stretching.

ability of field-induced two-bond dissociation, P_{sym}, is ~0.61. We assumed that the wave packet propagates in the lowest adiabatic state of CO_2^{2+}. Compared to the single ω-frequency case, P_{one} increases and P_{sym} decreases. More interesting is the asymmetry of the one-bond dissociation channels $O^+ + CO^+$ (R_1 dissociation) and $CO^+ + O^+$ (R_2 dissociation) as shown in Figure 9 by a snapshot of the wave packet at $t = 67.8$ fs for $\phi = (\pi/2)$. For $\phi = (\pi/2)$, the probability for R_1 dissociation is $P_1 \approx 0.34$ and the probability for R_2 dissociation is $P_2 \approx 0.05$. For the choice of the opposite phase, i.e., $\phi = -\pi/2$, P_1 and P_2 are interchanged with each other. As expected from the asymmetric shape of the cycle-averaged potential as shown in Figure 9 (dotted contour lines), one of the two C−O bonds is selectively dissociated in a two-color field of ω and 2ω.

6. Concluding Remarks

In this paper, we presented the results of theoretical investigation of structural deformations of CO_2 and its cations in a near-infrared intense field and showed that the experimentally observed structure of CO_2^{3+} ($R \approx 1.7$ Å and $2\theta \approx 20°$) just before Coulomb explosions originates from the structural deformation of CO_2^{2+}. It is concluded that the experimentally observed structure deformations occur when the molecular axis is parallel to the polarization direction of the field. In the CO_2 and CO_2^+ stages, ionization occurs before the field intensity becomes high enough to deform the molecule. Although the dissociation energy of CO_2^{2+} in a zero field is ~11 eV in the case of symmetric two-bond stretching and is ~1 eV in the case of one-bond stretching, simultaneous two-bond stretching occurs as well as one-bond stretching. Two-bond stretching is induced by an intense field in the lowest time-dependent adiabatic state $|1\rangle$ of CO_2^{2+}, and this two-bond stretching is followed by the occurrence of a large-amplitude bending motion mainly in the second lowest adiabatic state $|2\rangle$ nonadiabatically created at large internuclear distances $R \approx 1.6$ Å by the field from $|1\rangle$. The potential shape of $|2\rangle$ is dominated by the field-free first excited state of CO_2^{2+}, of which the equilibrium geometry is a bent one owing to the strong Renner−Teller effect. The present example is the first demonstration of the effect of field-induced nonadiabatic transition in a polyatomic molecule.

We proposed that the experimentally observed two-body breakup to $CO^+ + O^+$ is due to the one-bond stretching in the CO_2^{2+} stage. The probability of two-body breakup is smaller in the adiabatic transition case than in the vertical transition case where one-bond stretching initially occurs. In an alternating field whose frequency is larger than the vibrational frequencies, two-bond stretching is more field-induced than is one-bond stretching. This is due to the disappearance of the odd order terms with $\epsilon(t)$ in the cycle-averaged potential $\bar{V}_{x,1}(R_1,R_2,t)$ of CO_2^{2+}. As the field intensity approaches $I \approx 3.5 \times 10^{14}$ W cm^{-2}, the two-bond stretching becomes dominant; at higher intensities, the two-bond stretching becomes unbound. The appearance of field-induced two-bond stretching is also ascribed to the features of $\bar{V}_{x,1}(R_1,R_2,t)$ characteristic of the molecular dynamics in near-infrared, intense fields; in CO_2^{2+}, the stabilization energy $-\alpha(R_1,R_2)f(t)^2/4$ due to the induced dipole moment is large around the ridge of $R_1 = R_2$ relative to the dissociation energy for two-bond stretching. Since a similar structural deformation to that in the CO_2 case is reported for CS_2,[32] the proposed mechanism of dynamics of CO_2 in intense fields is presumably typical of the dynamics of linear triatomic molecules.

It is well-known that there is an approach to treat dynamics in intense fields, namely, the Floquet (dressed state) method targeted for long-time pulses with a constant envelope.[55] In the Floquet method, a molecule-field state is given by a product of a photon state and an adiabatic state in a zero field denoted by $|N - l\rangle$ and $|\Phi_j\rangle$, respectively. Here, N is the number of photons before the interaction and l is the number of photons absorbed by the molecule; the corresponding field-dressed *diabatic* potential is given by $\hbar\omega(N - l) + E_j(\{R\})$. The field-dressed *diabatic* states can be obtained by diagonalizing the R-fixed Hamiltonian including the molecule-field interactions among diabatic field-dressed states. This approach is especially useful for estimating the momenta of fragment ions and is now applicable to short pulses with a time-varying envelope.[56] From a practical point of view, however, the range of its application is rather limited to simple diatomic molecules such as H_2^+.[56,57] In this approach, it is necessary to calculate all of the field-free adiabatic states involved in the process under consideration (including *high-lying* states) and, moreover, the field-free states obtained are then dressed with photon number states. The number of photons absorbed or emitted, l, can be much larger than 1. Application of the Floquet approach to polyatomic molecules is therefore a very laborious process. On the other hand, the present time-dependent adiabatic state approach has the advantage that only a small number of *low-lying* adiabatic states that can be efficiently calculated by MO methods are required to describe the electronic and nuclear dynamics of a

(55) Shirley, J. H. *Phys. Rev.* **1965**, *138*, B979−B987. Chu, S.-I. *Adv. At. Mol. Phys.* **1985**, *21*, 197−253.
(56) Sugawara, M.; Kato, M.; Fujimura, Y. *Chem. Phys. Lett.* **1991**, *184*, 203−208. Day, H. C.; Piraux, B.; Potvliege, R. M. *Phys. Rev. A* **2000**, *61*, 031402(R)1-4.
(57) Muller, H. G.; Backsbaum, P. H.; Schumacher, D. W.; Zavriyev, A. *J. Phys. B* **1990,** *23*, 2761−2769.

molecule in intense laser fields. It should be pointed out that many field-free excited states are involved even in the lowest adiabatic state $|1\rangle$.

We have demonstrated that the concept of the cycle-averaged potential is also useful for designing schemes to control molecular dynamics, e.g., cleavage of chemical bonds, in intense fields. We theoretically predict that one of two C−O bonds can be selectively dissociated by a *nonresonant* two-color field of ω and 2ω. A foreseeable application of the present approach is simulation of the control of more complex processes, such as chemical reactions of polyatomic molecules in intense fields.[3,4,58] The dynamics of CO_2 presented in this paper suggests that control of chemical reactions in intense fields should be carried out in a manner that Coulomb explosions occurring at large internuclear distances are avoided. It is of great importance to examine how a desired reaction product is selectively created by manipulation of field-induced nonadiabatic transitions which are ubiquitous in the case of polyatomic molecules.

Acknowledgment. We thank Professors K. Yamanouchi and A. Hishikawa for their valuable discussions. This work was supported in part by a grant-in-aid for scientific research (No. 14540463) and a grant-in-aid for scientific research on priority areas, "Control of Molecules in Intense Laser Fields" (Area No. 419) from the Ministry of Education, Science and Culture, Japan.

JA0344819

(58) Ohtsuki, Y.; Sugawara, M.; Kono, H.; Fujimura, Y. *Bull. Chem. Soc. Jpn.* **2001**, *74*, 1167−1191.